Advances in the Optimization and Form-finding of Tensegrity Structures

Session Organizer: Gunnar TIBERT (KTH, Royal Institute of Technology)

Keynote Lecture
Optimal tensegrity structures in bending
Robert SKELTON, Mauricio de OLIVEIRA (University of California, San Diego)*

Reciprocal diagrams and stress control of tensegrity systems
Andrea MICHELETTI (University of Rome "Tor Vergata")

Bending-stiff tensegrity masts: Do they exist?
Gunnar TIBERT (KTH, Royal Institute of Technology)*

A tensegrity catalogue using point group theory
R. PANDIA RAJ, Simon D. GUEST (University of Cambridge)*

Form finding analysis of tensegrity membrane structures based on variational method
Mizuki SHIGEMATSU, Masato TANAKA, Hirohisa NOGUCHI (Keio University)*

Tensegrity architecture calculation of the cellular cytoskeleton
Bernard MAURIN, Patrick CAÑADAS, René MOTRO (Université Montpellier 2)*

For multiple-author papers:
Contact author designated by *
Presenting author designated by underscore

Proceedings of the 6th International Conference on
Computation of Shell and Spatial Structures
IASS-IACM 2008: "Spanning Nano to Mega"
28–31 May 2008, Cornell University, Ithaca, NY, USA
John F. ABEL and J. Robert COOKE (eds.)

Optimal tensegrity structures in bending

Robert SKELTON*, Mauricio de OLIVEIRA

*University of California San Diego
MAE Dept, 9500 Gilman Dr, La Jolla, CA 92093-0411
bobskelton@ucsd.edu

1 Abstract

This paper provides the closed form analytical solution to the problem of minimizing the material volume required to support a given set of bending loads with a given number of discrete structural members, subject to material yield constraints. The solution is expressed in terms of two variables, the aspect ratio, ρ^{-1}, and complexity of the structure, q (the total number of members of the structure is equal to $q(q+1)$). The minimal material volume (normalized) is also given in closed form by a simple function of ρ and q, namely, $V = q(\rho^{-1/q} - \rho^{1/q})$. The forces for this nonlinear problem are shown to satisfy a linear recursive equation, from node-to-node of the structure. All member lengths are specified by a linear recursive equation, dependent only on the initial conditions involving a user specified length of the structure. The final optimal design is a class 2 tensegrity structure. Our results generate the 1904 results of Michell [1] in the special case when the selected complexity q approaches infinity. Providing the optimum in terms of a given complexity has the obvious advantage of relating complexity q to other criteria, such as costs, fabrication issues, and control. In fact, when the number of joints are penalized in the volume criterion (to represent joint mass or fabrication costs), the optimal structural complexity is ***finite***, and indeed quite small. Hence, only simple structures (small q) are needed for practical design.

2 Minimal Mass for Structures in Bending

Complex structures are composed of components that are either under tensile loads, or compressive loads, or bending loads. For efficient designs it would be useful to know what kind of structural subsystems are efficient under each type of load. A second kind of efficiency in design is to assure that the members are *uni-directionally* loaded. A structural system in which the loads in any member never reverse direction allows for efficient choice of materials.

There are two approaches to design material systems in which the members are uni-directionally loaded. The first is to *prestress* the structure to reduce the *variety* of member loads that the structural members can experience.

The second approach to achieve uni-directional loading of discrete members is to choose a special *topology* of the set of members (the geometrical arrangements), coordinated with the given set of expected loading conditions. The two freedoms of prestressability (the amount of tension to pre-set in the members) and topology (the geometrical freedom in arranging material) offer great opportunities in the optimization process to arrange simple components for *uni-directional* loading during the loaded operation of the structure. We will take the second approach (topology optimization) and find, for a given wide range of external forces and directions, and a specified number of discrete material members (which we relate to a complexity figure of merit 'q'), a minimal volume of material which also satisfies yield constraints.

We define a *tensegrity system* as a prestressable connection of rigid bodies, such that the rigid bodies impart only forces (not torques) at their connections [2, 3].

It is convenient to make note of the number of rigid bodies that are connected. We define a *class-k tensegrity*

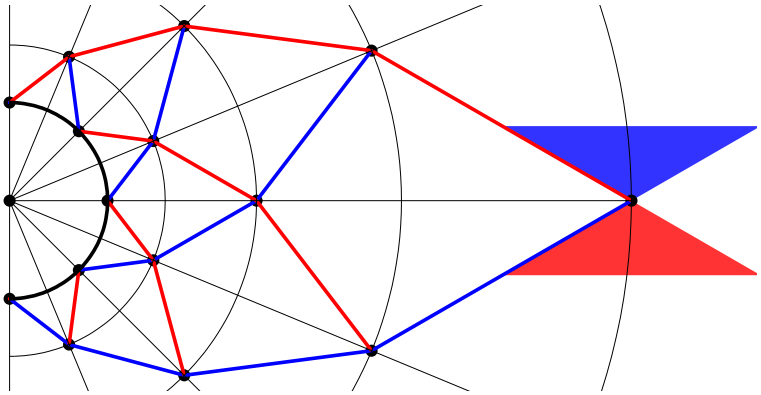

Figure 1: Michell Topology of Order 4 ($q = 4$, $\phi = \pi/16$, $\beta = \pi/6$) showing bending region; blue and red indicate a member in compression or tension.

system as a tensegrity system such that no more than k rigid bodies make connections at a given node (with frictionless ball joints). The word prestressable here refers to the fact that tension in the strings is required to stabilize the structure to hold any given shape. Notice also that the class k distinction refers to the arrangement of the rigid bodies and has nothing to do with the arrangement of strings, save the assumption that strings can indeed be arranged to stabilize the structure. Obviously, from this definition a *class*-1 *tensegrity*, contains rigid bodies that do not touch each other.

If there are no shape constraints on the rigid body design, it is not uncommon to use the simplest rigid body for the compressive members, namely rods. This suits the problem we examine in this paper, structures that are optimal in bending.

We enlarge Buckminister Fuller's definition of tensegrity, which was too imprecise for scientific work. Within the framework of our class-k definitions above, the word *tensegrity* coined by Buckminister Fuller describes what we have labeled *Class 1 tensegrity* systems, since the rigid rods did not touch in the designs made popular in the artworks of Ioganson and Snelson.

The most important reference in this paper is the seminal work of Michell in 1904 [1], where he showed a continuum of material to minimize volume for material system under bending loads, under the assumption that all members use the same materials. (Michell's optimization result requires that all members are composed of the same material, as first pointed out by [4, 5]). This is commonly called today the *Michell Truss*.

This paper gives a discrete optimal result for beams in bending, whereas Michell's 1904 results [1] provided only the continuum solution.

3 Contributions of the Paper

This paper provides the complete analytical solution for the design of a planar cantilevered structure with a circular foundation to support a given bending load, using the smallest volume of material required to support the load, while satisfying constraints against material yielding. The specific properties of the new results are itemized for clarity below.

The "complexity" q relates to the number of members ($= q(q+1)$) in the *Michell Topology*, as the one shown in Fig. 1. The relevant parameters, the radii r_ℓ, $\ell = 0, 1, \ldots, q$ and member lengths p_ℓ, $\ell = 0, 1, \ldots, q-1$, and the angles β and ϕ are defined with respect to a single *Michell Spiral* of order (complexity) $q = 4$ in Fig. 2.

The number $\rho^{-1} = r_0/r_q$ represents an aspect ratio for the structure. The radius r_0 is the length of the structure from reference point $\mathbf{0}$ and r_q is the radius of the circular foundation boundary.

A class-2 tensegrity truss structure (herein called a *Michell Topology*) has been studied. We have shown that the properties of such structures are completely characterized as a function of its complexity (q) and the aspect ratio of the structure (ρ^{-1}).

From node to node, the forces within the structure propagate according to linear recursive equations. We derived analytic formulas to compute the static equilibrium forces under arbitrary load scenarios.

In the case of a single external load applied at the node $\mathbf{n}_{00}$, we have shown that for a very large variation in the direction of the load the members experience forces in a single direction, either tensile or compressive, regardless of the magnitude of the external load, the complexity q or the aspect ratio ρ^{-1}. In such configuration the Michell

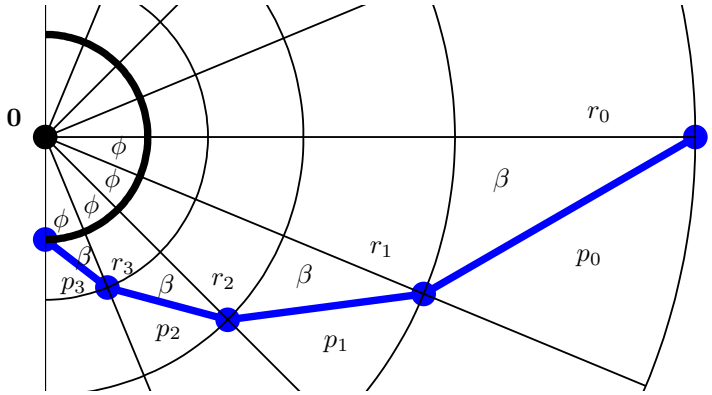

Figure 2: A Michell Spiral of Order 4 ($q = 4$, $\phi = \pi/16$, $\beta = \pi/6$)

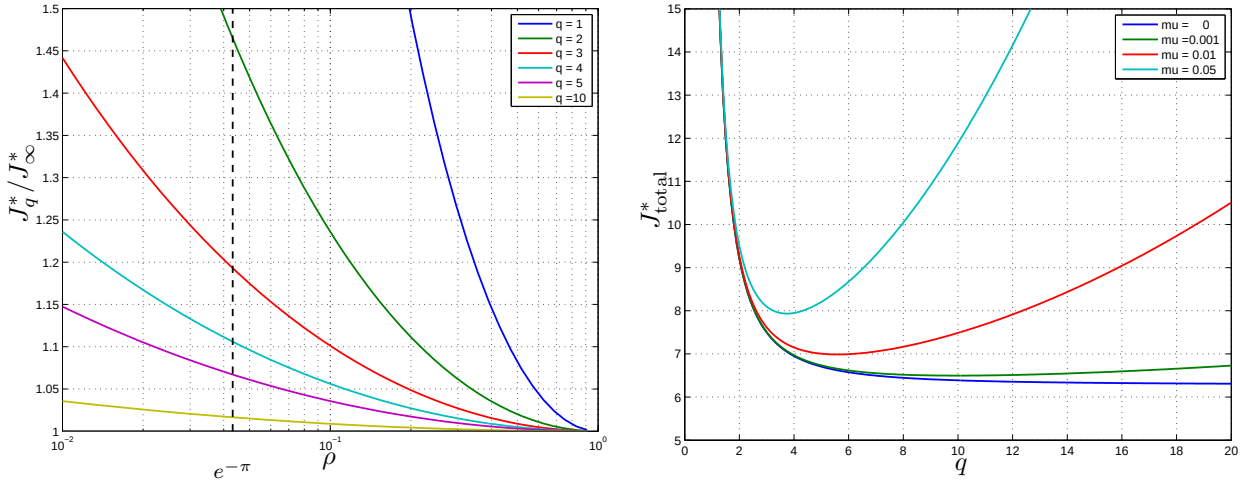

Figure 3: The relative optimal discrete cost J_q^*/J_∞^*; material overlap occurs for $\rho \leq e^{-\pi}$; The joint mass optimal discrete cost J^*_{total} plotted for the worst case $\rho = e^{-\pi}$.

Topology is a class-2 tensegrity structure. In Fig. 1, the shadded area represent the directions of th external load that put the Michell Topology in bending.

Under the assumption that the maximum tensile and compressive stresses are the same, we analyzed the total material volume subject to a yielding constraint. We showed that the minimal volume of material (normalized by some constant) is proportional to the simple quantity $J_q^* = q(\rho^{-1/q} - \rho^{1/q})$. As in [1], the optimal material topology depends on neither material choice nor magnitude of the load, if the direction of the applied load lies within a specified (large) range.

The results give the optimal design for any fixed complexity q, but the minimum volume of material occurs at infinite complexity ($q \to \infty$), in the absence of any mass added in fabricating joints. The optimal discrete cost J_q^* is compared with the optimal continuum design J_∞^* in the first plot of Fig. 3. If the mass of the joints is considered the optimal structural complexity is finite, and indeed quite small, as shown in the second plot in Fig. 3. (More about this issue later.)

The angle between the connecting tensile and compressive members approaches 90 degrees ($\beta^* \to \pi/4$) in the limit as the complexity q approaches infinity. This agrees with the infinitely complex results (filling the space with a material continuum) of Michell [1], where the intersection of tensile and compressive stress lines are always at 90 degrees. In our finite-complexity (discrete) results the angle between tensile and compressive members ($2\beta^*$) is optimized and is always less than 90 degrees. In fact the tangent of the optimal β^* is simply $\rho^{1/q}$, where $\rho \in [0, 1]$. The optimal angles β^* and the total wrapping angle $q\,\phi^*$ are shown in Fig. 4.

Ignoring joint mass, as in the above discussions, the optimal structural complexity is $q = \infty$, yielding the material continuum of Michell. However, even if joint mass is ignored, very low complexity produces a material volume close to the continuum optimum. The optimized material volume is within 7% of the continuum solution

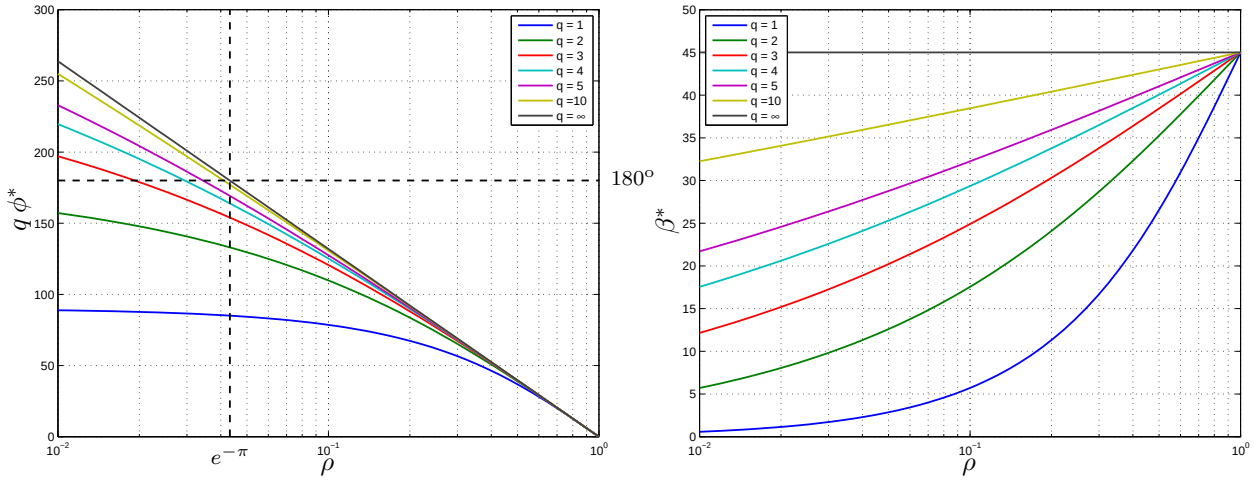

Figure 4: The optimal total angle $q\,\phi^*$ and departure angle β^* (in degrees); material overlap occurs for $\rho \leq e^{-\pi}$

when $q \geq 5$ and within 2% when $q \geq 10$.

Practically, increasing complexity q to large values does not yield improved design, since other neglected issues (such a fabrication errors, material inhomogeneities, ignored fasteners, glue mass, etc.), will have more effect than the suboptimality due to the use of a finite q. We quantify this effect by adding to the structural volume objective function a mass (volume) penalty in proportion to the number of joints. We assume that the volume of the joints is proportional to the number of joints $q(q+1)$, so the new criteria to optimize is $J_{new} = q(\rho^1/q - \rho^{-1/q} + \mu q(q+1))$, where μ is the ratio of joint mass to the mass of the members being joined. Hence $\mu = 0.001$ would suggest that the joint mass is 0.1 percent of the mass of the member being joined. Note that a fairly clean joint ($\mu = 0.001$) yields an optimal complexity at around $q = 10$. Sloppy joints, require a very low optimal complexity of $q = 3$, or $q = 4$. Such fabrication effects are characterized to show that if the joint mass is within 0.1 percent of the mass of the members being joined, then there is an optimal complexity at $q = 10$. More massive joints lead to less complexity for the optimal structure.

The interested reader is referred to the journal version of this paper [6].

References

[1] A. G. M. Michell, "The limits of economy of material in frame-structures," *Philosophical Magazine*, vol. 8, pp. 589–597, 1904.

[2] R. E. Skelton and M. C. de Oliveira, *Dynamics and Control of Tensegrity Structures*. Springer-Verlag, 2008. To be published.

[3] R. Skelton, "Dynamics and control of tensegrity systems," in *Proceedings of the IUTAM Symposium on Vibration Control of Nonlinear Mechanisms and Structures* (H. Ulbrich and W. Günthner, eds.), (Munich, Germany), pp. 309–318, Springer, 2005.

[4] G. I. N. Rozvany, "Some shortcomings in Michell's truss theory," *Structural Optimization*, vol. 12, pp. 244–250, Dec. 1996.

[5] G. I. N. Rozvany, "Some shortcomings in Michell's truss theory - author's reply and corrigendum," *Structural Optimization*, vol. 13, pp. 203–204, Apr. 1997.

[6] R. E. Skelton and M. C. de Oliveira, "Optimal tensegrity structures in bending: The discrete Michell truss." Submitted for publication to *Structural and Multidisciplinar Optimization*.

Proceedings of the 6th International Conference on
Computation of Shell and Spatial Structures
IASS-IACM 2008: "Spanning Nano to Mega"
28–31 May 2008, Cornell University, Ithaca, NY, USA
John F. ABEL and J. Robert COOKE (eds.)

Reciprocal diagrams and stress control of tensegrity systems

Andrea MICHELETTI*

*Department of Civil Engineering - University of Rome "Tor Vergata"
Via Politecnico 1, 00133, Rome, Italy
micheletti@ing.uniroma2.it

Abstract

We show that reciprocal diagrams can be found also for three-dimensional self-stressed frameworks, like tensegrity systems. Since the axial forces and edge-lengths of a system are respectively equal to the edge-lengths and axial forces of the corresponding reciprocal system, the self-stress in a tensegrity system can be controlled by applying a suitable form-finding procedure to the reciprocal.

1 Reciprocal diagrams

Reciprocal diagrams were first introduced by Maxwell [4] in the 19^{th} century for the graphical static analysis of two-dimensional frameworks. Reciprocal diagrams are related to projections of polyhedral surfaces and have numerous usages (see the introduction in Orden *et al.* [7] and the literature cited therein). A modern application can be found in Block and Ochsendorf [1].

In this section we reformulate the duality between edge-lengths and axial forces in self-stressed pin-connected frameworks. Figure 1 (left) depicts both a structure and its representation as an oriented graph. If the four nodes lay on the same plane, this structure has a single self-stress state, represented in Figure 1 (center); thicker lines in the graph corresponds to compressed edges.

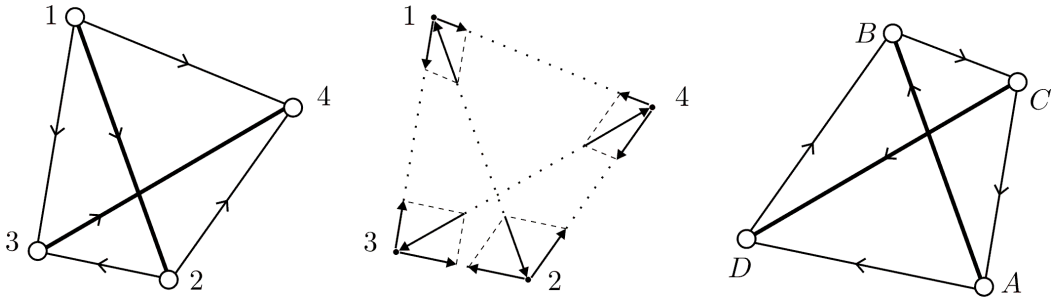

Figure 1: A structure with planar graph (left) and its self-stress state (center). The corresponding reciprocal system (right).

We use latin and greek subscripts respectively for quantities related to the nodes and the edges of the system; we can also denote an edge by the ordered pair of nodes it connects. If the oriented graph has n nodes and e edges, the incidence matrix is a n by e matrix whose (i, α) entry, $c_{i\alpha}$, can be defined as

$$c_{i\alpha} = \begin{cases} 1 & \text{if edge } \alpha \textit{ exits} \text{ node } i \\ -1 & \text{if edge } \alpha \textit{ enters} \text{ node } i \\ 0 & \text{if edge } \alpha \text{ is not incident on node } i \end{cases} . \tag{1}$$

The incidence matrix for the graph in Figure 1 (left) is written as follows:

n\e	12	13	14	23	24	34
1	1	1	1	0	0	0
2	−1	0	0	1	1	0
3	0	−1	0	−1	0	1
4	0	0	−1	0	−1	−1

. (2)

Notice that each column of this matrix has exactly two nonzero entries which are equal to 1 and -1, consequently, the row vectors sum up to the null vector in $\mathbb{R}^e$.

We denote by $\boldsymbol{e}_\alpha \in \mathbb{R}^3$ the unit vector parallel to the direction of edge α, with same orientation. If t_α is the axial force, or *stress*, carried by edge α, positive if the edge is in traction, then the equilibrium equation of node i, under no external force, is written as

$$\sum_\alpha c_{i\alpha} t_\alpha \boldsymbol{e}_\alpha = \boldsymbol{0}\,. \tag{3}$$

In graph theory, the row space of the incidence matrix is called the *bond space*, or *cut space*, a subspace of $\mathbb{R}^e$. Considering a row of the incidence matrix, if we remove from the graph the edges which correspond to the non-zero entries, we obtain two disconnected subgraphs, one of which is constituted by a single node. The orthogonal complement of the cut space in $\mathbb{R}^e$ is called the *cycle space*. A basis of the cycle space for our system is given by the three row vectors of the following matrix:

	12	13	14	23	24	34
A	1	−1	0	1	0	0
B	−1	0	1	0	−1	0
C	0	1	−1	0	0	1

. (4)

It is easy to check that the scalar product of each row of this matrix with any row of the incidence matrix is zero. Each element of the basis represents a *cycle* in the graph, that is a closed path with non repeating edges. For example, the first row vector in (4) correspond to the cycle $1 \to 2 \to 3 \to 1$, where edges (1,2) and (2,3) have the same orientation with respect to that of the cycle, while edge (1,3) has opposite orientation.

The complementarity of the cut space and the cycle space is one of the keys to the duality between two systems. The basis in (4) has been chosen in a way such that *each edge appears at most in two cycles* and *the orientations of an edge as it appears in two cycles are opposite to each other*. To the matrix in (4), we can add another row vector which is the sum of the three rows changed in sign. In this way, we obtain the following matrix which has the form of an incidence matrix:

n\e	(12) AB	(13) CA	(14) BC	(23) AD	(24) DB	(34) CD
A	1	−1	0	1	0	0
B	−1	0	1	0	−1	0
C	0	1	−1	0	0	1
D	0	0	0	−1	1	−1

. (5)

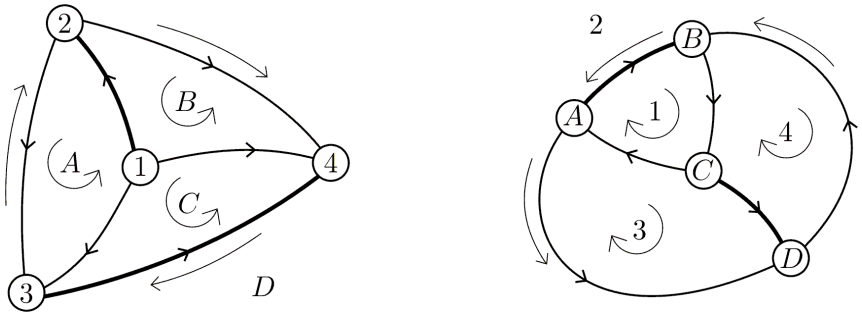

Figure 2: The dual planar graphs corresponding to the dual structures in Figure 1.

A choice of the basis for the cycle space which satisfies the above requirements is possible if and only if the graph is *planar*, i.e. the graph can be drawn on the paper without edge intersections. Figure 2 shows the two planar graphs associated to the dual incidence matrices (2) and (5).

We denote by $c^*_{i\alpha}$ the (i, α) entry of the matrix in (5). If ℓ_α is the length of edge α, then for each cycle we have the relation

$$\sum_\alpha c^*_{i\alpha} \ell_\alpha \boldsymbol{e}_\alpha = \mathbf{0}\,, \tag{6}$$

which has the same form of the equilibrium equation (3). This correspondence leads to the following result in the planar case: there exists a non-null self-stress state if and only if there exist a dual or *reciprocal* structure with lengths ℓ^*_α and unit vectors $\boldsymbol{e}^*_\alpha$, which satisfy

$$\sum_\alpha c_{i\alpha} \ell^*_\alpha \boldsymbol{e}^*_\alpha = \mathbf{0} \quad \forall\, i\,, \tag{7}$$

$$\boldsymbol{e}^*_\alpha = \pm \boldsymbol{e}_\alpha \quad \forall\, \alpha\,. \tag{8}$$

The cycle space and cut space are exchanged in the two systems. Corresponding edges are parallel to each other. The unit vectors which correspond to compressed elements have opposite orientation:

$$\begin{cases} \boldsymbol{e}^*_\alpha = \boldsymbol{e}_\alpha & \text{if } \ t_\alpha > 0\,, \\ \boldsymbol{e}^*_\alpha = -\boldsymbol{e}_\alpha & \text{if } \ t_\alpha < 0\,. \end{cases} \tag{9}$$

In absolute value, the stresses t^*_α and the lengths in the dual structure are respectively equal to the lengths and stresses in the primal structure:

$$\begin{cases} |t^*_\alpha| = \ell_\alpha\,, \\ \ell^*_\alpha = |t_\alpha|\,. \end{cases} \tag{10}$$

Edges with stresses of opposite sign have dual stresses of opposite sign, so that

$$\sum_\alpha c^*_{i\alpha} t^*_\alpha \boldsymbol{e}^*_\alpha = \mathbf{0} \quad \forall\, i\,. \tag{11}$$

Figure 1(right) shows the dual structure in this example.

Although originally the duality between stresses and lengths was considered valid only for system in two dimensions, is it clear from the above formulation that it also holds for three-dimensional system, as long as their underlying graph is planar. This result can be generalized to non-planar graph, as we will show in a following paper.

2 Stress control

Once the correspondence between the stresses in a system and lengths in its reciprocal has been established, various form-finding methods already developed for tensegrity systems can be applied to the reciprocal system, in order to find a convenient self-stress in the original one. Among these methods (for a recent review, see Hernandez Juan and Mirats Tur [3]), a suitable procedure is the one established by Williams [8], and successively developed by Micheletti and Williams [5, 6]. This method is based on the characterization of the *rank-deficiency manifold*, which is the set of placements of a structure for which the equilibrium matrix has rank r not maximal. During a motion on the manifold, the vector of nodal velocities have to remain on the tangent plane to this manifold.

Starting from a given rank-deficient placement, a change in shape is obtained by using edge-lengths as control parameters in compatibility equations, *i.e.* those equations which give the stretching velocity of the edges as a function of the nodal velocities. Compatibility equations and tangential conditions form together a system of ordinary differential equations which can be solved efficiently with the Runge-Kutta integration scheme. In this way the rank of the equilibrium matrix stays the same, the system remain in a self-stressed state and the lengths of the system can be directly controlled.

Figure 3 shows the result of the application of this procedure to the reciprocal of a classic tensegrity system, starting from a cyclic-symmetric configuration. Notice that after the transformation the lengths of the original system (Figure 3, top left) are all different from each other. To prescribe shape and self-stress of a system at the same time, it is necessary to apply the procedure simultaneously to both the system and its reciprocal, with additional conditions to maintain the duality relationship.

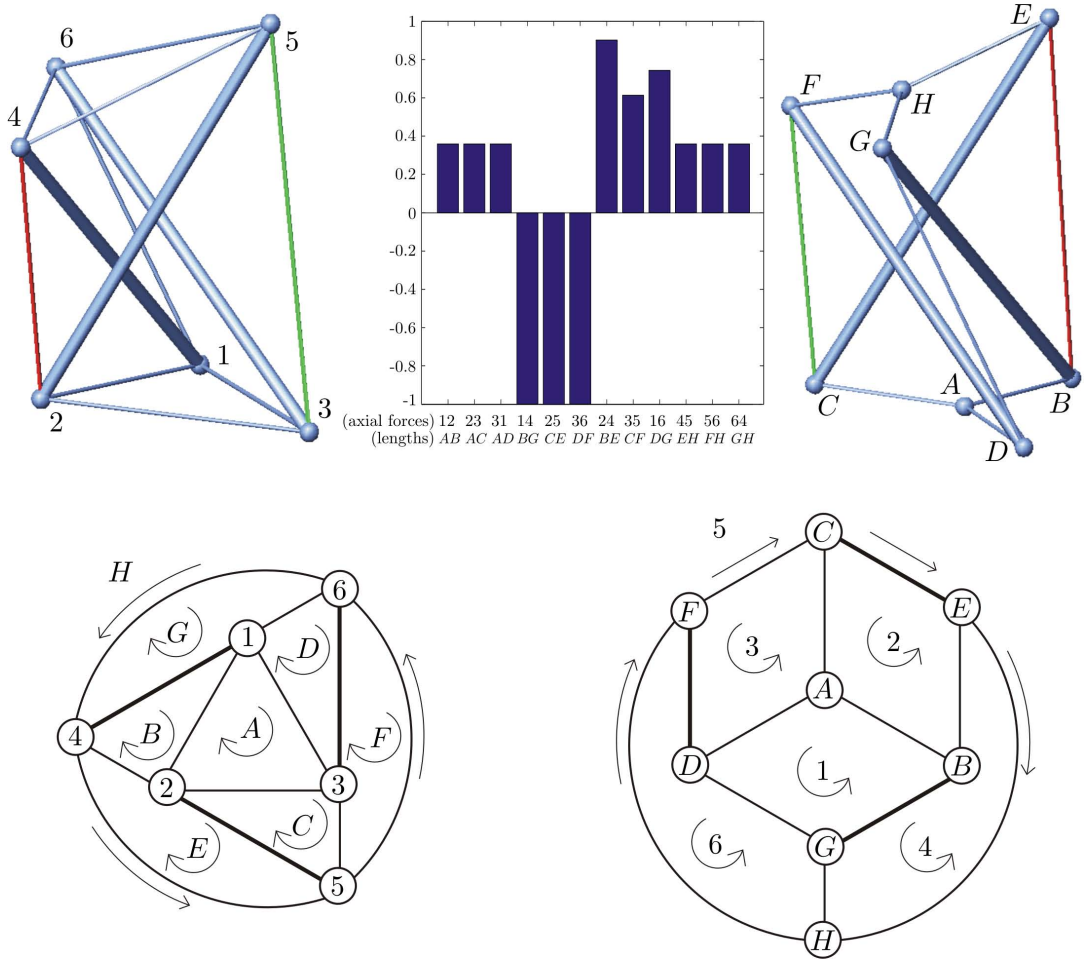

Figure 3: A tensegrity structure (top left) and its reciprocal (top right). Starting from a cyclic-symmetric configuration, the lengths of two edges in the reciprocal have been changed. The bar plot (top center) represents lengths and stresses of the two systems. The two corresponding planar graph are shown at the bottom.

References

[1] Block P and Ochsendorf J. Thrust network analysis: a new methodology for three-dimensional equilibrium. *Journal of the International Association for Shell and Spatial Structures* 2007; **48**:167–173.

[2] Bondy JA and Murty USR. Graph Theory with Applications. Elsevier: New York, 1976.

[3] Hernandez Juan S and Mirats Tur JM. Tensegrity frameworks: static analysis review. *International Journal of Mechanism and Machine Theory* (in press) available online 14 August 2007.

[4] Maxwell JC. On reciprocal figures and diagrams of forces. *Philosophical Magazine* 1864; **4**:250–261.

[5] Micheletti A and Williams WO. A marching procedure for form-finding of tensegrity systems. *Journal of Mechanics of Material and Structures* 2007; **2**:857–882.

[6] Micheletti A and Williams WO. Shape-change of tensegrity systems by controlling edge-lengths. In *Proceedings of IASS Symposium 2007*. University IUAV of Venice, Venice, 2007.

[7] Orden D, Rote G, Santos F, Servatius B, Servatius H, Whiteley W. Non-crossing frameworks with non-crossing reciprocals. *Discrete and Computational Geometry* 2004; **32**:567–600.

[8] Williams WO. A Primer on the Mechanics of Tensegrity Structures. Scientific report, Department of Mathematical Sciences, Carnegie Mellon University, Pittsburgh PA, 2003.

Proceedings of the 6th International Conference on
Computation of Shell and Spatial Structures
IASS-IACM 2008: “Spanning Nano to Mega”
28–31 May 2008, Cornell University, Ithaca, NY, USA
John F. ABEL and J. Robert COOKE (eds.)

Bending-stiff tensegrity masts: Do they exist?

Gunnar TIBERT*

*KTH Mechanics, Royal Institute of Technology
Osquars backe 18, SE-10044 Stockholm, Sweden
tibert@kth.se

Abstract

In an attempt to understand the cause of the low bending stiffness of tensegrity mast with discontinuous compression members, tensegrity structures with vertical and horizontal compression members are studied.

1 Introduction

The tensegrity concept is interesting for the design of deployable structures for space and terrestrial applications due to the relatively few number of compressive elements, which makes folding easy. An automatic and reliable deployment approach for large tensegrities is still to be found, but more important is that the deployed structure has high stiffness and strength. This is presently not the case for slender tensegrities with discontinuous compression members (Class I tensegrity) [8]. To achieve the adequate stiffness of large scale structures, one finds that continuous compression members (Class II tensegrity) cannot be avoided. A recent example is the design of the Rostock Messeturm by Schlaich, Bergermann & Partner [6]. Continuous struts may be accepted for non-deployable applications, but from a deployability viewpoint discontinuous struts are desirable as they are the key to simplicity in manufacturing and creation of small stowed volumes.

2 Conventional truss masts versus tensegrity masts

Truss booms for space applications typically have three longerons connected by transverse battens and diagonals. Recent studies [2, 4, 5] show that the truss boom designs are highly optimised in terms of bending stiffness and strength as most material in the boom are positioned away from the centroid. In comparison, the most unfortunate characteristic of a tensegrity structure is that the compression members are inside the structure, passing through the centroid. Like for a cable formed by helical wires around a straight centre wire, the alignment of the struts decreases the axial stiffness of the mast. Masic et al. [3] optimise the stiffness of a two-stage Snelson-type mast and find, as expected, that the hexagonal saddle cable between the two stages becomes a triangle, i.e. the struts are no longer discontinuous. Hence, stiffness optimisation of a tensegrity with discontinuous struts leads to a configuration with continuous struts. As noted by Masic et al. [3], this is to be expected as the compressive load path becomes shorter for Class II tensegrities. The paths of compressive stresses for different mast are schematically compared in Figure 1. It is clear that the compressive stresses has to go from the compressive side of the truss to the tensile side of the truss in the case of a tensegrity mast. This means that the cables on the compressed side slackens and the full integrity of the tensegrity is lost. Further load increase leads to more slack cables and consequently less bending stiffness [8].

Thus, the idea here is to investigate if a tensegrity mast with vertical and horizontal struts, like a truss mast, will be stiffer than a tensegrity mast with crossing struts.

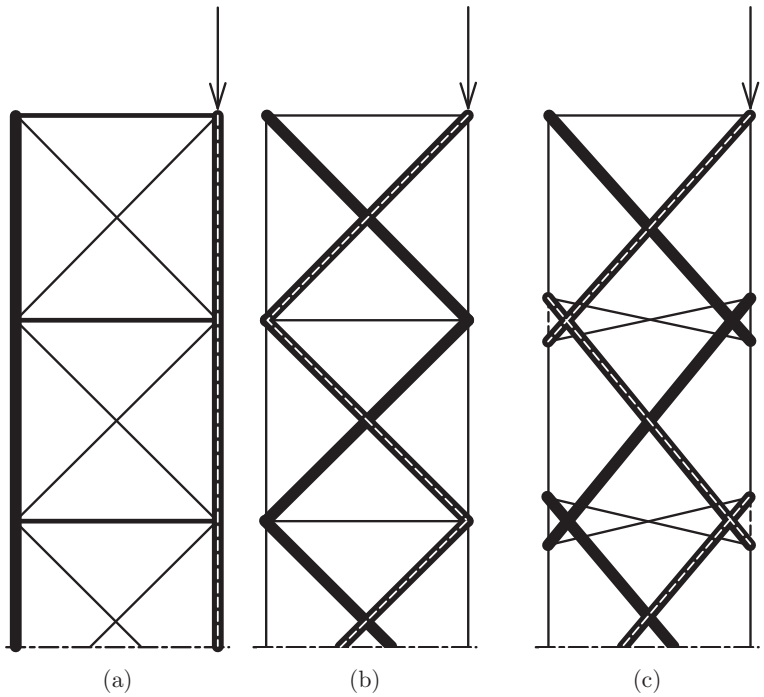

Figure 1: Schematic view of the force flow (dashed lines) through a truss mast (a) and tensegrity masts with continuous (b) and discontinuous struts (c).

3 Two-dimensional masts with vertical struts

To test the idea that vertical struts separated by horizontal struts will create a more stiff mast, a suitable tensegrity module must be found. This is first done in two dimensions. Three different tensegrity modules are shown in Figure 2, where the version in (c) is most suitable since it can be prestressed more easily than the (b) version. The possibility of using the module in Figure 2(c) as a building block to create tensegrity masts with discontinuous struts was tested by a trial-and-error approach using the generalised Maxwell's rule. This resulted in the mast shown in 3(d). The stiffness of this mast was then compared to other two-stage masts by means of flexibility ellipsoids, Figure 3. A flexibility ellipsoid shows the displacement at a node due to a unit force oriented in any direction. Flexibility ellipsoids provide an easy way of visually comparing the stiffness of trusses. The truss mast is very stiff in its axial direction and so is the tensegrity with vertical struts. However, the proposed vertical-strut tensegrity is weaker in bending than the cross-strut tensegrities. Unexpectedly, the cross-strut tensegrities have comparable stiffnesses, although it is generally known that the strut discontinuity often significantly weakens the structure in bending. The most likely explanation is that the two stage mast here is in only two dimensions and not very slender.

From this simple analysis of two-dimensional masts, it appears that the introduction of vertical struts creates higher axial stiffness, but not higher bending stiffness.

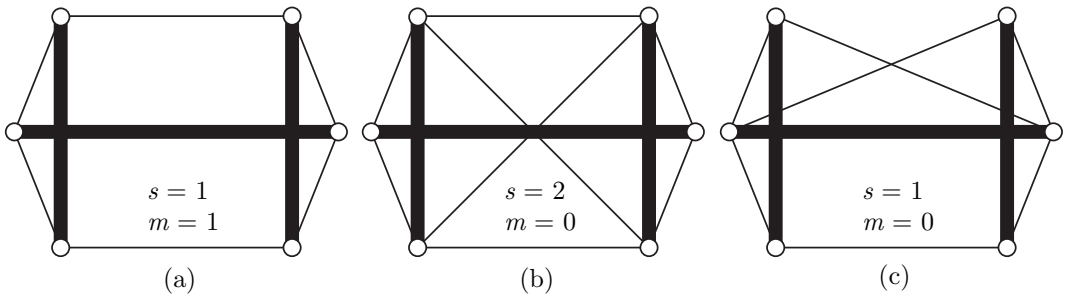

Figure 2: Various tensegrity modules with vertical struts.

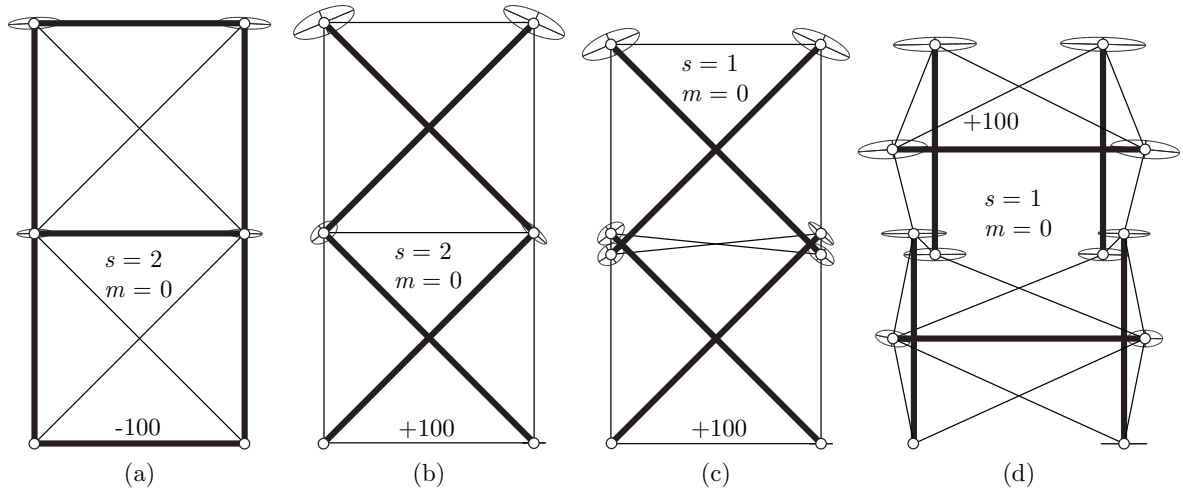

Figure 3: Comparison of the stiffness of different two-stage masts: (a) truss, (b) continuous cross-struts tensegrity, (c) discontinuous cross-struts tensegrity and (d) vertical struts tensegrity.

4 Three-dimensional masts with vertical struts

Analyses of two-dimensional tensegrities can yield initial results, but analysis of three-dimensional structures are required, since the topology and geometry are often much more complex in three dimensions. A comparison of two-stage tensegrity masts with continuous and discontinuous struts in terms of initial stiffness is shown in Figure 4. The masts seem to have similar stiffness: the stiffening effects of the continuous struts are weakened by the two mechanisms, $m = 2$. Hence, in terms of initial stiffness, a mast discontinuous struts is not always weaker than one with continuous struts.

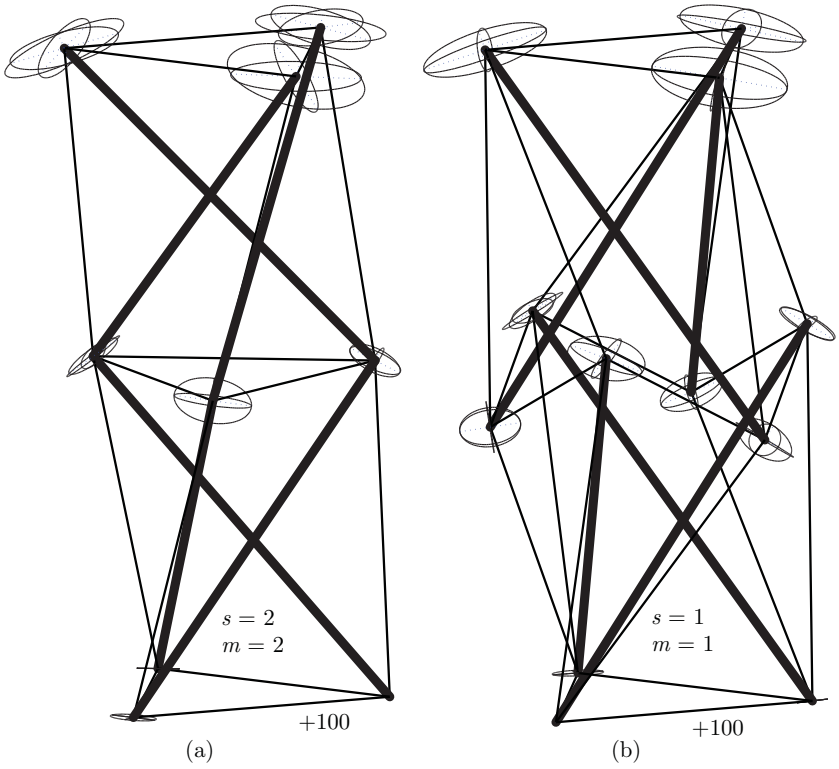

Figure 4: Comparison of the stiffness of three-dimensional two-stage masts: (a) continuous and (b) discontinuous struts.

To create a three-dimensional mast with vertical struts, the two-dimensional modules in Figure 2(b) and (c) are extended in the third dimension. These three-dimensional versions are shown in Figure 5. The more simple one, (a), is actually more complex with ten states-of-selfstress and two mechanism. Several trials were made to create multi-stage masts using this module and although the resulting masts did not contain any mechanisms, they contained several states-of-selfstress with no admissible combination of them. Not surprisingly, module (b), which has better static and kinematic properties, is identical to the sculptures *Sound box* and *X-tend* built by Kenneth Snelson in 1966–67 [7]. More surprisingly though is that this module is statically determinate and thus not prestressable. Still, it may be useful as a building block to create tall masts if a suitable topology is found.

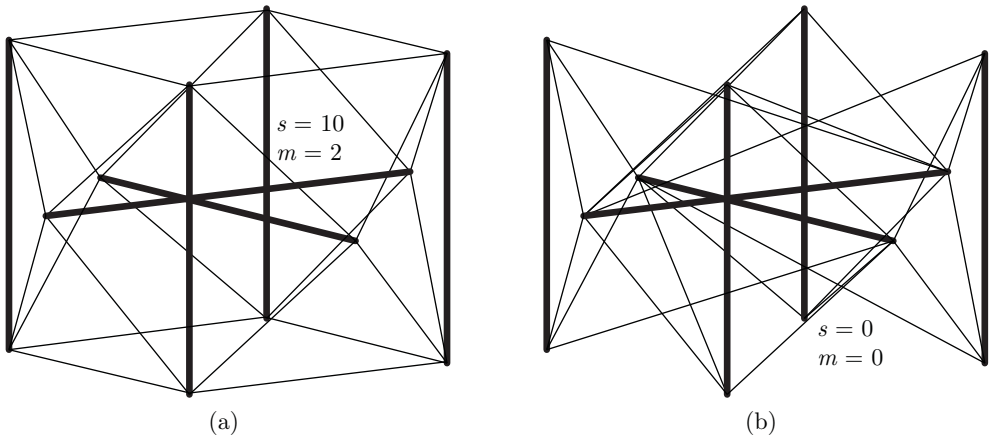

Figure 5: Three-dimensional tensegrity modules with vertical struts.

5 Conclusions

The aim of this study was to investigate if a reorientation of the discontinuous compression members to vertical and horizontal orientations is a key to a higher bending stiffness of slender masts. A two-dimensional example indicates that this might not be the case: the axial stiffness increases, but the bending stiffness decreases compared to tensegrity masts with crossing compression members. A tensegrity by Snelson has been proposed for the design of three-dimensional masts with vertical and horizontal struts.

References

[1] De Jager B, Skelton RE. Stiffness of Planar Tensegrity Truss Topologies. *International Journal of Solids and Structures* 2006; **43**:1308–1330.

[2] Greschik G. Truss Beam with Tendon Diagonals: Mechanics and Design. *AIAA Journal* 2008; **46**:557–567.

[3] Masic M, Skelton RE, Gil PE. Optimization of Tensegrity Structures. *International Journal of Solids and Structures* 2006; **43**:4687–4703.

[4] Mikulas MM, Collins TJ, Doggett W, Dorsey J, Watson J. Truss Performance and Packaging Metrics. In *Proceedings of Space Technology and Applications International Forum*, Albuquerque, NM, USA, February 12–16, 2006.

[5] Murphey TW. Booms and Trusses. In *Recent Advances in Gossamer Spacecraft*. AIAA Progress in Astronautics and Aeronautics, Vol. 212, 2006.

[6] Schlaich M. The Messeturm in Rostock—A Tensegrity Tower. *Journal of the IASS* 2004. **45**:93–98.

[7] Snelson K. `http://www.kennethsnelson.net`, Online Internet, March 15, 2008.

[8] Tibert G. *Deployable Tensegrity Structures for Space Applications*. PhD thesis, Stockholm, Sweden. 2002.

Proceedings of the 6th International Conference on
Computation of Shell and Spatial Structures
IASS-IACM 2008: "Spanning Nano to Mega"
28–31 May 2008, Cornell University, Ithaca, NY, USA
John F. ABEL and J. Robert COOKE (eds.)

A tensegrity catalogue using point group theory

R. Pandia Raj, S.D. Guest*
*University of Cambridge
Department of Engineering
Trumpington Street, Cambridge, CB2 1PZ, UK
sdg@eng.cam.ac.uk

Abstract
We show how applied point group theory can be used to generate the tensegrity catalogue that was originally produced by Connelly and Back, and suggest some simple extensions of the catalogue.

1 Introduction

Tensegrity structures are remarkable in that they frequently do not have enough members to satisfy Maxwell's rule for the rigidity of frameworks, and yet they are stable structures. Commonly the compression members (struts) are not directly connected to one another, and are connected only by a network of tension members (cables).

The key to the stability of tensegrity structures is their *geometric*, or *second-order* stiffness, which can be conveniently described using a *stress matrix* (Guest [4]). For three-dimensional structures, if the stress matrix has a nullity of four, and positive semi-definite eigenvalues, then the structure is said to be *super-stable*, meaning that the structures is guaranteed to be stable (if we exclude the pathological cases where affine motions leave member lengths unchanged (Schenk *et al.* [6])). As we shall see in section 2, the stress matrix also plays a key role in finding equilibrium configurations for tensegrities.

Connelly and Back [3] generated a catalogue of symmetric tensegrity structures using the following assumptions for each structure, that: (1) the structure belonged to some symmetry group (2) there would be a single *regular orbit* of nodes; (3) there would be a single *orbit* of struts; and (4) there would be two *orbits* of cables. An orbit of nodes (struts or cables) implies that, starting with one node (strut or cable), each symmetry operation would shift that node to coincide with another node (strut or cable) in the same orbit. A *regular* orbit of nodes implies that a different node will be generated by each symmetry operation.

Connelly and Back generated their catalogue by considering the permutation symmetries of the nodes of their structures, i.e., how the nodes were swapped by symmetry operations. Here, we revisit their catalogue by instead considering the point group symmetry of the structure, i.e., we consider each symmetry operation as being a rotation (proper or improper) or a reflection. This allows us to connect Connelly and Back's work with ongoing work to recast structural ideas in symmetry-adapted form, to provide an alternative explanation of how the catalogue is generated, and to explore how the catalogue might be extended.

Our basic approach is as follows. Like Connelly and Back, we assume that there is a regular orbit of nodes (each can be considered as corresponding to one symmetry operation), one orbit of struts, and two orbits of cables. However, unlike Connelly and Back, we choose in advance the point group symmetry of the tensegrities that we are trying to find: in our catalogue they may have icosahedral, cubic, or tetrahedral symmetry. For each possible choice of cables and struts, we look for equilibrium configurations by ensuring that the stress matrix is rank deficient by at least 4. It turns out to be straightforward to do this in terms of the 3×3 irreducible representation matrices that correspond, for each symmetry operation, to the transformations of the x, y and z coordinates of a node. Once the equilibrium configuration has been found, it can then be checked for stability and accepted if it is a stable configuration, or rejected otherwise. It turns out that many choices of cables and struts give stable tensegrities.

2 Form-finding

Our approach to form-finding for tensegrity structures in the catalogue is described in Pandia Raj and Guest [5]. The basic question is the choice of *tension coefficient* (internal force divides by length) for each member, such that a super stable structure can exist. Consider a tensegrity structure containing n nodes. For a given set of tension coefficients in the members, we define an $n \times n$ *stress matrix* $\mathbf{S}$ (also known as a force density matrix) as follows. Consider two nodes i and j, possibly connected by a member ij which has a tension coefficient $\hat{t}_{ij}$. The coefficients of the stress matrix are then

$$\mathbf{S}_{ij} = \begin{cases} -\hat{t}_{ij} & \text{if } i \neq j, \\ \sum \hat{t}_{ik} & \text{if } i = j : \text{summation over all nodes } k \text{ connected to node } i \\ 0 & \text{if } i \text{ and } j \text{ are not connected} \end{cases} \tag{1}$$

If this stress matrix has a nullity of four (for 3D structures), with positive semi-definite eigenvalues, then it corresponds to a super-stable tensegrity, and the coordinates of the nodes can be found from any three independent vectors, $\mathbf{x}$, $\mathbf{y}$ and $\mathbf{z}$, in the nullspace of $\mathbf{S}$. The n-dimensional vectors $\mathbf{x}$, $\mathbf{y}$ and $\mathbf{z}$ then contain, respectively, the x, y and z coordinates of each of the n nodes.

The stress matrix for tensegrities in the catalogue can be written in a particularly simple way. The first thing that we do is choose a reference, or identity node, which we label E. Then every node corresponds to one of the symmetry operations g in the symmetry group G, and we can label every node with the corresponding symmetry operation. Similarly, we label a member connecting node E with node g as member g, carrying tension coefficient $\hat{t}_g$. Secondly, we note that corresponding to each symmetry operation g is a *permutation matrix* $\mathbf{P}_g$, which describes how the nodes are rearranged by the symmetry operation. Then it can be shown that the stress matrix defined in equation (1) can also be written as a weighted sum of the permutation matrices:

$$\mathbf{S} = \sum_g \left\{ (\mathbf{P}_E - \mathbf{P}_g) + (\mathbf{P}_E - \mathbf{P}_{g^{-1}}) \right\} \hat{t}_g, \tag{2}$$

where the summation is taken over all operations g where a member connects nodes E and g. (There is an awkwardness of definition here if $g^{-1} = g$, for instance when g is a reflection operation, as the tension coefficient appears twice in equation (2) when it should only appear once — but we can get around this by defining $\hat{t}_g$ as *half* the tension coefficient in this case.)

Although the stress matrix has a simple formulation, finding values of tension coefficients in the members that give the correct nullity can be difficult; but it is greatly assisted by writing everything using a symmetry-adapted coordinate system.

3 Symmetry-adapted form-finding

Pandia Raj and Guest [5] show how, for any symmetric tensegrity, it is possible to find a symmetry-adapted coordinate system that greatly simplifies the finding of tension coefficients that give the stress matrix the correct nullity. Using this symmetry-adapted coordinate system, the stress matrix takes a block diagonal form, $\tilde{\mathbf{S}}$, and equation (2) takes the form:

$$\tilde{\mathbf{S}} = \sum_g \left\{ (\tilde{\mathbf{P}}_E - \tilde{\mathbf{P}}_g) + (\tilde{\mathbf{P}}_E - \tilde{\mathbf{P}}_{g^{-1}}) \right\} \hat{t}_g, \tag{3}$$

where $\tilde{\mathbf{P}}_g$ is a *block-diagonalised* permutation matrix.

In the current context, the remarkable feature of equation (3) is that we don't need to follow the method described by Pandia Raj and Guest [5] to find the block-diagonalised matrices. Because we know that we have a regular orbit of nodes, a basic result of group representation theory (see, for instance, Bishop [2]) is that the permutation matrices $\mathbf{P}_g$ form a *regular representation*, and have a known form in terms of *irreducible representation matrices*, which can either be straightforwardly derived, or read off from a book of group theory tables (Altmann and Herzig [1]).

A further simplifying feature for the present formulation is that it isn't even necessary to form the complete stress matrix in order to find suitable tension coefficients $\hat{t}_g$. Because we know that we are trying to find x, y, and z coordinates for a set of nodes that do not lie on symmetry elements (e.g. rotation axes, or planes of reflection), then we know that the nullity in $\tilde{\mathbf{S}}$ must arise from the particular irreducible representation matrices labelled xyz in Altmann and Herzig [1]; for the tetrahedral, octahedral or icosahedral tensegrities in Connelly and Back's catalogue, these are always 3×3 matrices. Thus finding tension coefficients to give a putative structure reduces to finding when a weighted sum of known 3×3 matrices is rank-deficient.

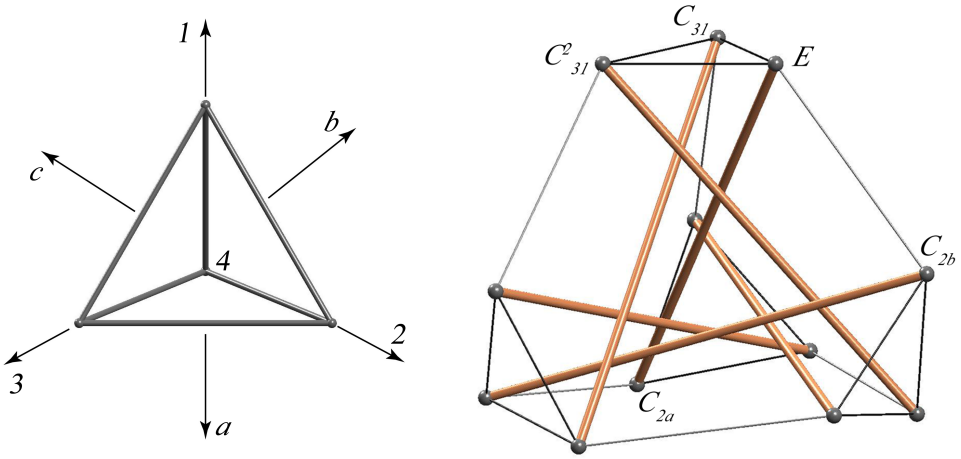

(a) (b)

Figure 1: (a) A tetrahedron showing 7 symmetry axes; four 3–fold rotational axes along the vertices of tetrahedron, 1, 2, 3 and 4, and three 2–fold rotational axes along the lines, a, b, and c. (b) An example tensegrity structure with T symmetry, i.e., the symmetries of rotations, but not reflections, of the tetrahedron shown in (a).

4 Example Structures

In this section we will show examples of tensegrity structures with point group symmetry T, the symmetries of rotations, but not reflections, of a tetrahedron (Fig. 1). Since this T group tensegrity structure originates from tetrahedron, this structure has 7 symmetry axes, which are along the vertices and vertex diagonals of tetrahedron. The twelve symmetry operations; the identity, E, rotations by 120° and 240° about the vertices, 1, 2, 3 and 4; $\{C_{31},\ C_{32},\ C_{33},\ C_{34},\ C^2_{31},\ C^2_{32},\ C^2_{33},\ C^2_{34}\}$, and rotation by 180° about the a, b, and c axes, $\{C_{2a}, C_{2b}, C_{2c}\}$, form the symmetry group of the example structure. These twelve symmetry operations constitute the symmetry group T. We assume one regular orbit of nodes: there are 12 nodes, which have one to one correspondence with the 12 symmetry operations.

If we choose to have: (1) a strut connecting node E to node C_{2a} with tension coefficient $\hat{T}_s$; (2) cables connecting nodes E to node C_{31}, and node $C^{-1}_{31} = C^2_{31}$ with tension coefficients $\hat{T}_t$; and (3) a cable connecting E to node C_{2b} with tension coefficients $\hat{T}_d$, then the method described in section 3 reduces to finding values of the tension coefficients that make the following matrix $\tilde{\mathbf{S}}$ singular:

$$\tilde{\mathbf{S}} = \begin{bmatrix} 2\hat{T}_t + 2\hat{T}_s & -\hat{T}_t & -\hat{T}_t \\ -\hat{T}_t & 2\hat{T}_t + 2\hat{T}_d + 2\hat{T}_s & -\hat{T}_t \\ -\hat{T}_t & -\hat{T}_t & 2\hat{T}_t + 2\hat{T}_d \end{bmatrix}. \tag{4}$$

The solution $\hat{T}_t/\hat{T}_s = \hat{T}_d/\hat{T}_s = -1.74$ gives the structure shown in Fig. 1(b).

Other choices of struts and cables may give other structure: for point group symmetry T, the complete set of possible stable tensegrities are shown in Fig. 2.

5 Conclusions

This paper describes an elegant technique based on applied point group theory for generating simple symmetric tensegrities. It has concentrated on the case where there is a single regular orbit of nodes, and has shown the possible stable tensegrities with point group symmetry T. We are currently applying the method to other symmetry groups, and extending the method to consider cases where there is a single, but not regular, orbit of nodes.

6 Acknowledgements

R. Pandia Raj gratefully acknowledges the support of the Gates Cambridge Trust.

References

[1] Altmann, S. L., Herzig, P. *Point-group theory tables* Oxford: Clarendon, 1994.

[2] Bishop, D.M. *Group Theory and Chemistry* Oxford: Clarendon Press, 1973.

[3] Connelly, R. and Back, A. Mathematics and tensegrity. *American Scientist* 1998; **86**:142–151.

[4] Guest, S.D. The stiffness of prestressed frameworks: a unifying approach. *International Journal of Solids and Structures* 2006; **43**:842–854

[5] Pandia Raj, R. and Guest, S.D. Using Symmetry for Tensegrity Formfinding. *Journal of the International Association for Shell and Spatial Structures* 2006; **47(3)**:245-252.

[6] Schenk, M., Guest, S.D., Herder, J.L. Zero Stiffness Tensegrity Structures. *International Journal of Solids and Structures* 2007; **44**:6569–6583.

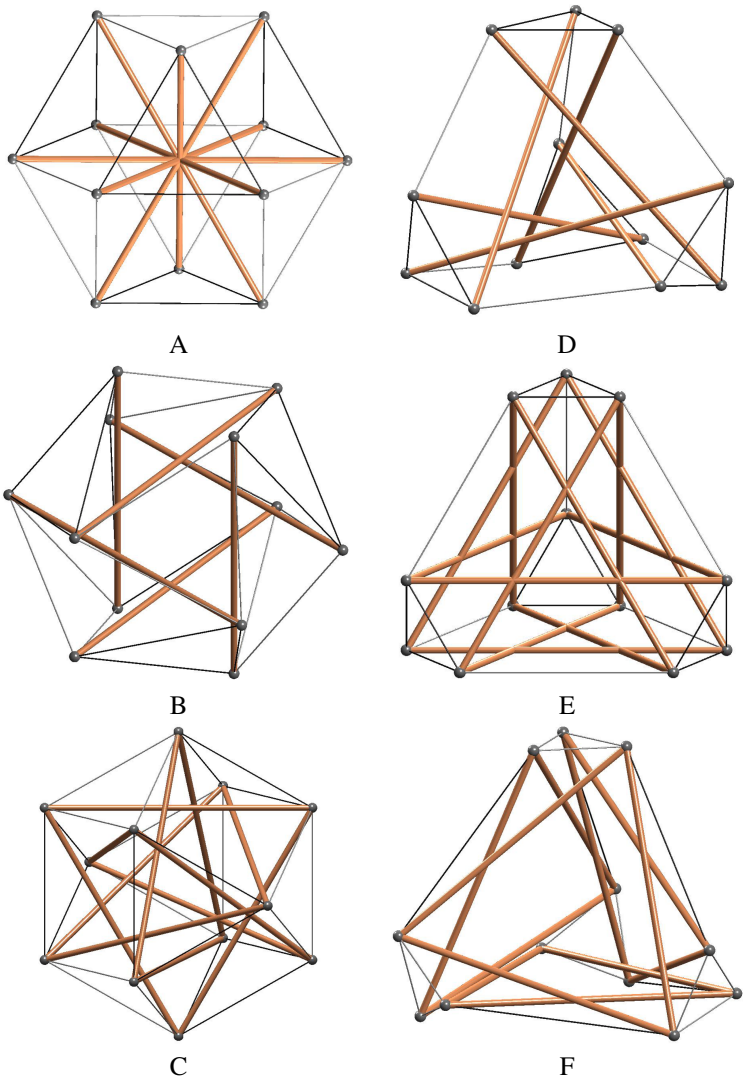

Figure 2: T group tensegrities. For each structure $\hat{T}_t/\hat{T}_s = \hat{T}_d/\hat{T}_s$, and this ratio is given by: (A) -1; (B) -0.67; (C) -1.5; (D) -1.74; (E) -3; and (F) -2.47

Proceedings of the 6th International Conference on
Computation of Shell and Spatial Structures
IASS-IACM 2008: “Spanning Nano to Mega”
28-31 May 2008, Cornell University, Ithaca, NY, USA
John F. ABEL and J. Robert COOKE (eds.)

Form finding analysis of tensegrity membrane structures based on variational method

Mizuki SHIGEMATSU*, Masato TANAKA, Hirohisa NOGUCHI

*School of Science for Open and Environmental Systems, Keio University
3-14-1, Hiyoshi Kohoku-ku, YOKOHAMA, 223-8522, Japan
mizuki@noguchi.sd.keio.ac.jp

Abstract

In this study, a “tensegrity membrane structure”, coupling tensegrity with a tensioned membrane structure, is presented. Firstly, through a static nonlinear finite element analysis, structural response is investigated to ensure that this structure can be established. Then, several tensegrity membrane structures are demonstrated to show that this present coupled structure could be more rational and universal than tensegrity or membrane structures themselves and might be referred to the next generation of space structures.

1. Introduction

R. Buckminster Fuller, a top rationalist of the 20th century, invented two rational structures, i.e. geodesic dome and tensegrity. These structures meet his demand of a “rational structure”. A rational structure achieves maximum space with minimum use of materials or in his words, "*Do more with less*". Tensegrity is a free-standing prestressed pin-jointed structure and the state of self-equilibrium is achieved by a combination of purely tensile or compressive loaded members under the absence of external loads and constraints. Tensegrity, however, does not cover spaces like membrane.

The feature of this study is that tension members are then replaced with an elastic membrane. Both tensegrity and membrane require “tension” to achieve the state of self-equilibrium and give stiffness to the structures. The present structure applies these tension loads to the elastic membrane in place of tension members, and finds a statically stable form with the state of self-equilibrium. This structure shall be referred to as a “tensegrity membrane structure”. It couples tensegrity with membrane via tension loads and can be one of the rational structures achieving maximum space with minimum use of materials.

2. Numerical Modeling of Tensegrity Membrane Structure

For modeling and designing a tensegrity membrane structure, an accurate and efficient numerical method is anticipated, however, to the best of the authors’ knowledge, there are few researches related to the tensegrity membrane structure. In this study, therefore, a novel form finding analysis of tensegrity membrane structure based on the variational method is presented, where compression struts and membranes are modeled with rigid elements and membrane elements respectively. The variational formulation is firstly derived to minimize the total potential energy of membrane elements with the constraint conditions to keep the length of rigid elements constant by using Lagrange multiplier method. Then, the virtual work principle for “tensegrity membrane structure” is obtained, and is solved by the nonlinear finite element method with the Newton-Raphson iterative scheme. With this technique, several simple structures of “tensegrity membrane structure” are investigated to find the respective statically stable form.

Equation (1) shows that the total potential energy of membrane with the constraint conditions for keeping the length of rigid elements constant.

$$\pi = \frac{1}{2}\int_V \boldsymbol{S} : \boldsymbol{E} dV + \sum_{i=1}^{n_b} \lambda_i \left(l_{Ri} - \bar{l}_{Ri} \right) \tag{1}$$

where π: total potential energy, $\boldsymbol{S}$: 2nd Piola-Kirchhoff stress tensor in membrane, $\boldsymbol{E}$: Green-Lagrange strain tensor in membrane, V : volume of membrane, l_R : distance of strut's end, $\bar{l}_R$: length of strut, λ : Lagrange multipliers (compression forces), n_b : total number of rigid struts

Taking the variation of total potential energy in Eq. (1), the virtual work principle can be derived as in Eq. (2):

$$\delta\pi = \int_V \boldsymbol{S} : \delta\boldsymbol{E} dV + \sum_{i=1}^{n_b} \lambda_i \cdot \delta\left(l_{Ri} - \bar{l}_{Ri} \right) + \sum_{i=1}^{n_b} \delta\lambda_i \cdot \left(l_{Ri} - \bar{l}_{Ri} \right) = 0 \tag{2}$$

In the present finite element procedure, the membrane is divided into triangular meshes and Eq. (2) can be discretized as in Eq. (3):

$$\begin{aligned} \delta\pi &= \sum_{e=1}^{n_e} \int_{V_e} \boldsymbol{S} : \delta\boldsymbol{E} dV_e + \sum_{i=1}^{n_b} \lambda_i \cdot \delta\left(l_{Ri} - \bar{l}_{Ri} \right) + \sum_{i=1}^{n_b} \delta\lambda_i \cdot \left(l_{Ri} - \bar{l}_{Ri} \right) \\ &= \left(\delta\boldsymbol{u}_1^T \cdots \delta\boldsymbol{u}_{n_p}^T, \delta\lambda_1 \cdots \delta\lambda_{n_b} \right) \begin{pmatrix} \boldsymbol{Q}_1 \\ \vdots \\ \boldsymbol{Q}_{n_p} \\ l_{R1} - \bar{l}_{R1} \\ \vdots \\ l_{Rn_B} - \bar{l}_{Rn_B} \end{pmatrix} = 0 \end{aligned} \tag{3}$$

Where $\boldsymbol{u}_1 \cdots \boldsymbol{u}_{np}$, $\boldsymbol{Q}_1 \cdots \boldsymbol{Q}_{np}$: the displacements and internal forces of each node, respectively, n_e and n_p: total number of membrane elements and nodes, respectively. It is a large deformation problem where high-order nonlinear equations are solved by using the Newton-Raphson method as in Eq. (4):

$$\Delta(\delta\pi) = \left(\delta\boldsymbol{u}_1^T \cdots \delta\boldsymbol{u}_{n_p}^T, \delta\lambda_1^T \cdots \delta\lambda_{n_b}^T \right) (\boldsymbol{K}) \begin{pmatrix} \Delta\boldsymbol{u}_1 \\ \vdots \\ \Delta\boldsymbol{u}_{n_p} \\ \Delta\lambda_1 \\ \vdots \\ \Delta\lambda_{n_b} \end{pmatrix} = \boldsymbol{R} \tag{4}$$

Here, $\boldsymbol{K}$ represents the tangent stiffness matrix and $\boldsymbol{R}$ the residual vector computed from the unbalanced nodal forces and length of struts.

3. Form Finding Analysis of Tensegrity Membrane

3.1 Analysis models and boundary conditions

There are three types of analysis models used in this paper, Diamond (Single Layer 4 prism), Diamond (Multi Layer) and Zigzag (Fullerene). They are modeled by membrane elements and rigid elements. For boundary conditions, only constraints to avoid rigid-body displacements and rotations are imposed.

3.2 Analysis of Diamond model: Single Layer 4 prism

Figure 1 shows the Diamond model: Single Layer 4 prism. A development (red: strut, black: membrane), an initial geometry of membranes, an analysis result after struts are added and a picture of real structure are displayed from the left.

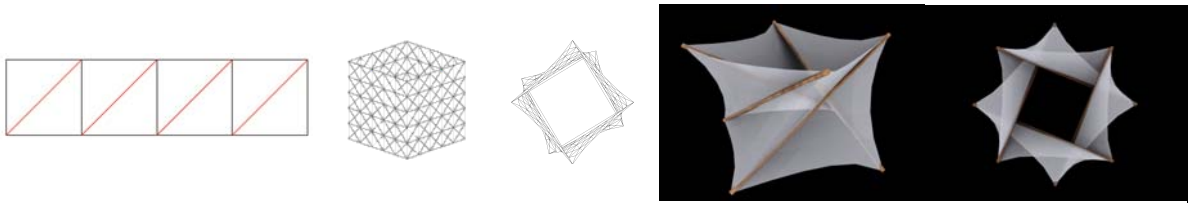

Figure 1: Single Layer 4 prism

3.3 Analysis of Diamond model: Multiple Layer

Figure 2 shows the Diamond model: Multiple Layer. A development (red: strut, black: membrane), an initial geometry of membranes, an analysis result after struts are added and a picture of real structure are displayed from the left.

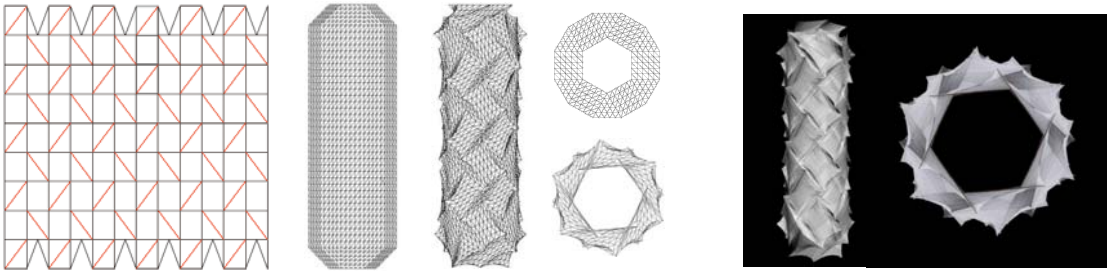

Figure 2: Multiple Layer

The tensegrity membrane structure designed in the next chapter was based on this model, where the model is cut into the half and the cutting plane faces on the ground.

3.4 Analysis of Zigzag model: Fullerene

Figure 3 shows the Zigzag model: Fullerene. A development (red: strut, black: membrane), an initial geometry of membranes, an analysis result after struts are added and a picture of real structure are displayed from the left.

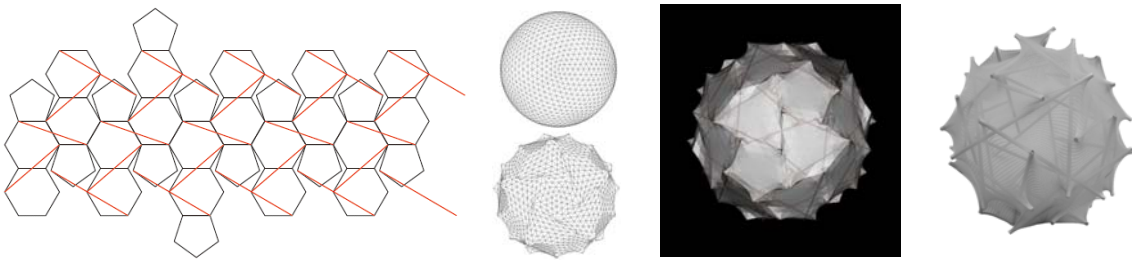

Figure 3: Fullerene

4. Design

Finally, as one of the application of tensegrity membrane structures, a tent warehouse near seaside has been designed and the possibilities of tensegrity membrane structure are shown. A tensegrity membrane structure could be adaptable for any kinds of sites, usages and scales, due to the feature of a lightweight, variform and rational structure.

4.1 Spatial design

Seen from the outside of the designed tent, there are many arches drawn as a frontline of membrane. Once one walks through the arch and into the tent, one sees that the mild lights, coming through the membrane, fall onto the open space with no columns. The struts seem to float in the air and it stimulates one's curiosity.

Figure 4: Spatial design using tensegrity membrane

4.2 Structural design

From the stress analysis of this designed tent warehouse, it is revealed that more flexible material for membrane is needed to realize tensegrity membrane structure without failure. Figure 5 shows the configuration and the contour of major stress after struts are added.

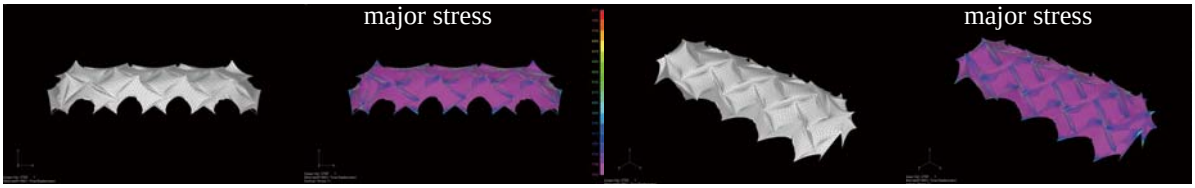

Figure 5: Structural design of tent warehouse

5. Conclusion

In this study, "tensegrity membrane" structure, coupling tensegrity with tensioned membrane structure, has been developed. By using the present analysis method, the self-equilibrium form of tensegrity membrane structure could be found and the basic configurations of Diamond and Zigzag models were demonstrated. The application to practical tent warehouse was also illustrated to show the possibilities of tensegrity membrane structure. Finally, this present coupled structure has been established as a novel rational structure.

References

[1] Hisada, T. and Noguchi, H., Basis and Application of Nonlinear Finite Element Method, MARUZEN, 1995, *in Japanese*.

[2] Goto, K, and Noguchi, H., Form Finding Analysis of Tensgrity Structures Based on Variational Method, Proceedings of CJK-OSM 4, 455-460, 2006.

Proceedings of the 6th International Conference on
Computation of Shell and Spatial Structures
IASS-IACM 2008: "Spanning Nano to Mega"
28-31 May 2008, Cornell University, Ithaca, NY, USA
John F. ABEL and J. Robert COOKE (eds.)

Tensegrity architecture calculation of the cellular cytoskeleton

Bernard MAURIN*, Patrick CAÑADAS, René MOTRO

*Laboratoire de Mécanique et Génie Civil
Université Montpellier 2 – Pl. Bataillon – CC48 – 34095 Montpellier cedex 5 - France
maurin@lmgc.univ-montp2.fr

Abstract

The biomechanical behavior of an adherent cell is strongly dependent on its cytoskeleton structure. Several models have been proposed to study it by taking into account its existing internal forces. However, the structural and geometrical complexities of the cytoskeleton's filamentous networks lead to difficulties for determining a biologically realistic architecture. We present a mechanical model and a numerical method devoted to the form-finding of the cytoskeleton structure when a cell adheres on a substrate. The cell is modeled as a granular medium and distant mechanical interactions mimic the cytoskeleton filament forces. The adhesion phenomenon is simulated by considering microtubules growing from the centrosome towards membrane receptors. This results in a compressive microtubule network and a corresponding tensile actin filament network, in interaction with the substrate reactions, therefore providing relevant shape and forces information exploitable in biomechanical studies of adherent cells using the tensegrity analogy.

1. Introduction

A main challenge of cellular biomechanics is to improve in the understanding of the relationships between the mechanical behavior of an adherent cell in interaction with its environment and its biological functions. Several experimental studies have allowed characterizing the mechanical response, but the heterogeneity and lack of quantitative coherence of the results emphasize on the necessity to develop a "general" cell mechanical modeling. The difficulty is however to model the behavior of the cytoskeleton (CSK) that plays an essential role by controlling both the shape and the mechanical response of adherent cells [4].

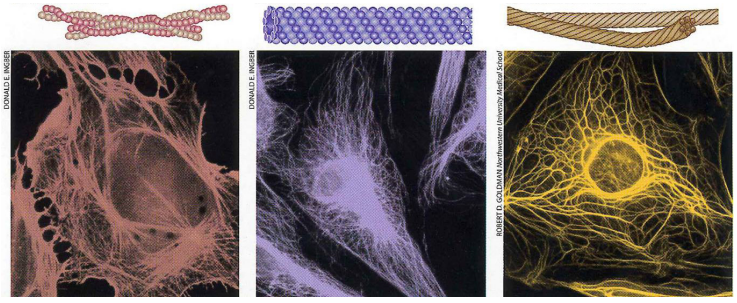

Figure 1: CSK filamentous networks

The CSK is composed of 3D structural complex networks of interconnected biopolymers (actin, microtubules and intermediate filaments, Figure 1) that ensure a physical linkage between the nucleus and transmembrane adhesion receptors. Its architectural organization depends on the mechanical interactions with the environment. Internal traction and compression forces carried by the CSK's filaments, which ensure the cell rigidity and stability, have been experimentally observed. In particular, actin filaments are tensioned in balance with compressed microtubules [6]. Among the models developed to describe the mechanics of adherent cells, those based on tensegrity systems have shown their pertinence by considering simultaneously the actin and

microtubule networks as well as the CSK's connection points. However, the complex and heterogeneous spatial distribution of filaments and forces is not taken into consideration enough realistically until now. Since these parameters mainly depend on the CSK structuration occurring during the cell adhesion process, our purpose is to develop a structural form-finding method to calculate a realistic prestressed structure, resulting from the cell adhesion and in equilibrium with the substrate reactions. The aim is to obtain a tensegrity-like structural model of the CSK, exploitable in future numerical simulations of the mechanical responses of adherent cells.

2. Tensegrity mechanical modeling of the CSK

2.1 Non regular tensegrity structures

The tensegrity structures used up today to analyze the CSK behavior are generally based on simple regular systems. The possibility to generate more complex and realistic structures has been however put forward at Montpellier University and a numerical method, based on dynamic relaxation, has been developed to generate irregular systems with more elements and various architectures [5] (Figure 2).

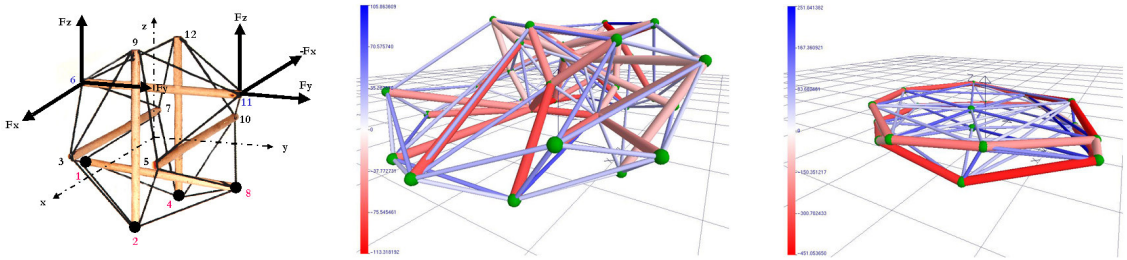

Figure 2: Regular tensegrity system (left); complex structures of epithelial (center) and platelet (right) cell

A main difficulty however remains for the calculation of biologically realistic CSK structures. Experimental observations may lead to several cues, as used for models presented in Figure 2, but are not easily exploitable to rebuild a complete 3D architecture. Since the CSK organization closely depends on the adhesion and spreading process of the cell on its substrate, we propose to model this process to determine the resulting filamentous networks. The approach is based on "granular tensegrity", based on divided-media mechanics, and consists in modeling the cell as a granular medium.

2.2 Granular tensegrity approach applied to cell mechanical modeling

This 3D approach consider a cell modeling as a discrete medium formed by an assembly of rigid spheres corresponding to intra-cellular cross-linking proteins (or "grains", Figure 3) with distant mechanical interactions representing the CSK filament internal forces. A central grain defines the nucleus and, all around, the cytoplasm is modeled by identical grains, two specific ones among them corresponding to the centrosome. The external plasma membrane is modeled by peripheral grains; some of them representing integrin adhesion receptors.

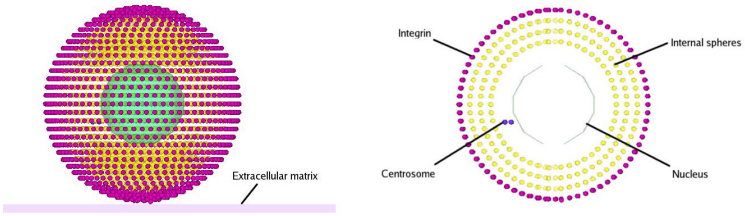

Figure 3: Cell granular model (initial non adherent state)

Before adhesion, the cell is spherical and the mechanical interactions are tacit (no internal forces, as for a cell in suspension). Every grain is connected to the neighboring ones by distant interactions, defined as elastic springs associated to the elasticity of actin and microtubules filaments, as considered in the tensegrity analogy. In the simulation, the shape of the cell is progressively modified until its complete adhesion and spreading, resulting in specific CSK's architecture and distribution of traction and compression forces.

2.3 CSK structuration process

Few details are currently available on the cell adhesion process and a simplified scenario had to be considered, consistent with biological assumptions [1]. We suppose that microtubules develop from the centrosome, grow then towards the substrate and push the integrins to adhere to the extra cellular matrix (Figure 4). The distances between grains change in this process and the cell geometry also. The elastic interactions result consequently in traction or compression forces, depending on the distance variations. The prestressed adherent structure then obtained characterizes an estimated architecture of the CSK with a specific distribution of tensioned actin filaments and compressed microtubules. It defines a complex tensegrity structure connected to the substrate. In the simulation, a microtubule is represented by a series of straight elastic segments connecting a path of grains and its growing is simulated by their step by step lengthening according to a tubulin polymerization speed.

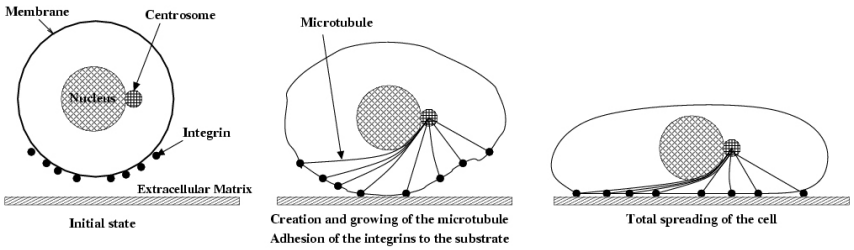

Figure 4: Simplified scenario for the cell adhesion process by microtubule polymerization

2.4 Substrate adhesion, adhesive reaction and numerical resolution

The adhesion between integrins and the extra cellular matrix is modeled by a sphere/plane contact. The adhesive laws are based on an extension of Signorini's contact and Coulomb's friction laws, depending to the normal distance between the substrate and an integrin grain. When contact is obtained, adhesion happens and an adhesive reaction results. A decohesion process occurs conversely up to a critical distance (broken junction). When contact takes place, in-plane tangential adhesive reaction forces become active to maintain the adhesion and avoid sliding. The "Non Smooth Contact Dynamics" method is used to solve the equations of mechanics. It allows considering dynamic adhesive contact and friction problem with a large number of grains. Non linearities due to contacts and to discontinuities of relative velocities are as well considered. The NSCD technique also allows specifying elastic distant interactions between grains to simulate the CSK's filaments.

3. Results

An application is presented using roughly 3400 grains, including 1150 for the plasma membrane, 40 for integrin receptors and 2 for the centrosome (located under the nucleus). Several steps of the cell adhesion and spreading processes are presented in Figure 5 when microtubules grow and push the integrin grains. In the first steps (top) the cell remains roughly spherical at the top while it begins to spread at the bottom. Spreading becomes then more and more significant and microtubules stretch the whole structure until the complete adhesion (bottom).

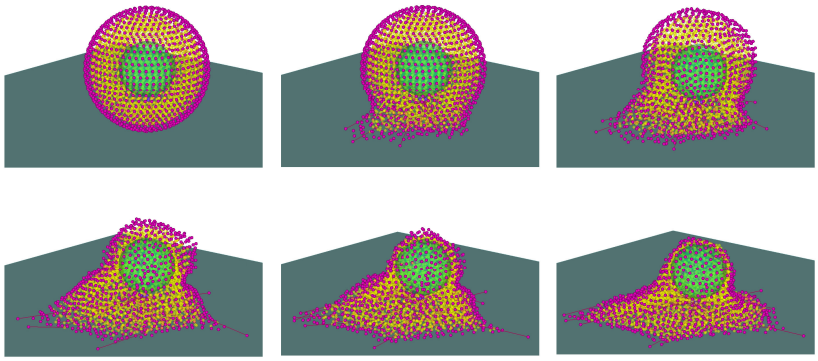

Figure 5: Computational steps of the cell adhesion and spreading

The resulting tensile network is shown in Figure 6. The most tensioned elements are basal, some of them on the edges and joining the integrin grains, while the less tensioned are on the apical face, consistently with in vivo observations of actin cortex and of basal stress fibers [3]. An experimental observation of an actin network is also presented as a comparison, showing these basal stress fibers noticeably on the cell edges [7].

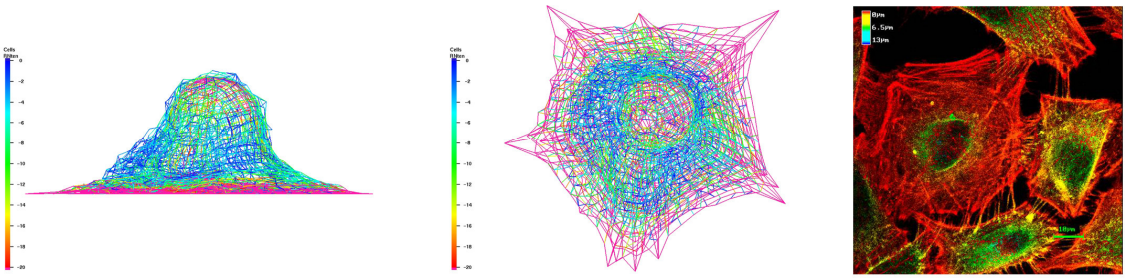

Figure 6: Actin tensile network (side view on the left, top view at centre) and confocal microscopy observation

The computed microtubule network is presented in Figure 7. They irradiate from the centrosome to the integrins ("star-like" shape), which fits with experimental observations for a PtK1 cell (on the right [2]).

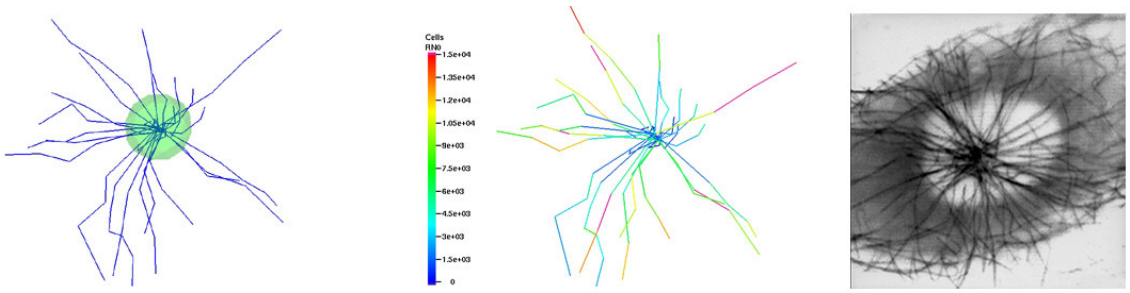

Figure 7: Compressive network (left and centre) and phase-contrast microscopy observation

4. Conclusion

The paper present a mechanical model and a numerical method devoted to the cytoskeleton form-finding resulting from its structuration during cell adhesion and spreading. We determine, by combining the tensegrity concept and the divided media theory, a more realistic CSK's structure than those used in classical models. The simulation considers a scenario of the cell adhesion based on the microtubule polymerization. This results in complex tensegrity-like structures relevant with biological observations.

References

[1] Goode BL, Drubin D, Barnes G. Functional cooperation between the microtubule and actin cytoskeletons. *Current Op. Cell Biol*. 2000; 12:63-71.

[2] Keating TJ et al. Microtubule release from the centrosome. *PNAS*. 1997; 94:5078-83.

[3] Laurent V, Fodil R, Cañadas P, Fereol S, Louis B, Planus E, Isabey D. Partitioning of cortical and deep cytoskeleton responses from transient magnetic bead twisting. *Ann. Biomed. Eng.* 2003; 31(10):1263-78.

[4] Matthews BD, Overby D, Mannix R, Ingber DE. Cellular adaptation to mechanical stress: role of integrins, Rho, cytoskeletal tension and mechanosensitive ion channels. *J. Cell Sci.* 2006; 119(3): 508-18

[5] Maurin B, Motro R, Baudriller H. Free-lengths tensegrity systems: conceptual design, form-finding and application, *Int. IASS Symp.: New Shells and Spatial Structures*, Beijing 2006:480-481.

[6] Stamenovic D, Mijailovic S, Tolic-Norrelykke I, Chen J, Wang N. Cell pre-stress II. Contribution of microtubules. *Am. J. Cell Physiol*. 2002; 282: C617-24.

[7] Wendling S et al. Stiffening response of a cellular tensegrity model. *J. of The. Biol*. 2000; 196 (3):309-25.